Overview of the Possibilities and Limitations of the Characterization of Ceramic Foam Filters for Metal Melt Filtration

Claudia Voigt, Jana Hubálková, Are Bergin, Robert Fritzsch, Ragnhild Aune, and Christos G. Aneziris

Abstract

The filtration of molten metal using ceramic foam filters (CFF) is a purification method often used by the aluminum industry to meet the increasing demands the melt quality. CFFs are in most cases produced by the replica method using polyurethane foam templates, which are coated with a ceramic slurry of targeted composition before being sintered into its final structure. Despite the key role of CFFs in view of metal cleanliness, there are only a few quality parameters for their evaluation. In the present study, an overview of the different material properties essential for CFFs, suitable measurement methods, and their limitations are presented. The focuses of this work are the different densities of ceramic foams and the thermal expansion coefficient measured by dilatometry, as well as the filter porosities and microstructure measured through mercury intrusion porosimetry and computer tomography, respectively. Moreover, elastic (Young's Modulus) and mechanical properties (compressive strength) are discussed.

C. Voigt (✉) · J. Hubálková · C. G. Aneziris
Institute of Ceramic, Glass and Construction Materials, Technische Universität Bergakademie Freiberg, Agricolastr. 17, 09599 Freiberg, Germany
e-mail: claudia.voigt@ikgb.tu-freiberg.de; Claudia.Voigt@ikfvw.tu-freiberg.de

J. Hubálková
e-mail: jana.hubalkova@ikgb.tu-freiberg.de

C. G. Aneziris
e-mail: aneziris@ikgb.tu-freiberg.de

A. Bergin · R. Fritzsch · R. Aune
Department of Materials Science and Engineering, Norwegian University of Science and Technology (NTNU), Trondheim, Norway
e-mail: are.bergin@ntnu.no

R. Fritzsch
e-mail: robert.fritzsch@ntnu.no

R. Aune
e-mail: ragnhild.aune@ntnu.no

Keywords

Filtration • Ceramic foam filter • Ceramic

Introduction

Ceramic foam filters are used for melt filtration of aluminum, iron, and steel since the 1960s [1, 2]. Despite the use of millions of ceramic foam filters every year, there are only a few specifications, guidelines, or papers about the requirements regarding the application as a metal melt filter. The properties specified in the BDG guideline (Bundesverband der Deutschen Gießerei—Industrie) [3] include several parameters, e.g. filter dimensions, tolerances for the filter dimensions, functional pore size, filter volume as well as measurement guidelines for the cold compressive strength, the amount of crumbs, and an impingement test.

In this study, an overview of "typical" and "untypical" measurable ceramic foam filter properties is presented, discussed, and the limitations of the possible measurements are described. These properties are explanatorily shown for a set of commercially available ceramic foam filters for continuous aluminum casting.

The mechanical properties of ceramic foams are often used to develop new filter compositions and for production quality control. The information about the mechanical properties is gathered by measuring compressive (or crushing) strength, bending strength, and Youngs Modulus, whereby the compressive strength is the most frequently measured mechanical property. Nevertheless, no standard for measuring the compressive strength of ceramic foams exists. Standards for measurement of the cold compressive strength of shaped insulating refractory products (DIN EN ISO 8895) [4] and dense shaped refractory products (DIN EN 993-5) [5] could be applied for the ceramic foam samples. These standards using samples with a size of $114 \times 114 \times 76$ mm^3 or $114 \times 114 \times 64$ mm^3,

© The Minerals, Metals & Materials Society 2021

L. Perander (ed.), *Light Metals 2021*, The Minerals, Metals & Materials Series,
https://doi.org/10.1007/978-3-030-65396-5_103

respectively, cylinders with a diameter of 50 mm and a height of 50 mm or cubes with 50 × 50 × 50 mm^3. But researchers and filter producers tend to use commercially available filter samples which result in a broad scope of sample geometries [6–10].

Voigt et al. [11] identified different parameters influencing the measured compressive strength, such as the size of the ceramic foam, the size of the loading plate, and the homogeneity of the foam. Due to the strong influence of the sample size, a direct comparison of samples with different geometries is not recommended by the authors. Measurements of Young's Modulus is a rarely used method for the characterization of ceramic foams, although it offers an opportunity to test, for example, the sinter progress. Grabenhorst et al. [12] determined the influence of the sample size and functional pore size of the ceramic foams on Young's Modulus measured by four different measuring methods: ultrasonic longitudinal method, the ultrasonic quasilongitudinal method, the impulse excitation method, and the three-point bending test method.

In the area of ceramic foam filters, it is necessary to distinguish between the different kinds of pores as well as different densities to prevent misunderstandings. There are three different kinds of pores based on manufacturing technology: the functional pores surrounded by struts, the strut cavities which are formed due to the decomposition of the polymeric foam, and the material pores within the struts [13, 14]. For the classification of ceramic foam filters regarding the size of the functional pores, which affects the filtration efficiency and the pressure drop, pores per inch (ppi) [15] or grades are used. Nevertheless, the use of the ppi classification is questionable because filters with the same ppi number can have different porosity by a variation of the strut thickness. It has to be noted that due to the dimensions of the polyurethane blocks during foaming of several meters, the pore size within one block varies resulting in different pore sizes for one given ppi number. Furthermore, there are differences in the functional pore size within the same ppi number between the different producers.

Furthermore, there are different kinds of densities which have to be used properly. The foam density ρ_{foam} is the bulk density of the whole ceramic foam (with the weight m and the volume V) calculated by

$$\rho_{foam} = \frac{m}{V} \tag{1}$$

and the relative density is defined as

$$\rho_{rel} = \frac{\rho_{foam}}{\rho_{solid}} \tag{2}$$

with the ρ_{solid} as the material density, which is the bulk density of the strut material. The true density is the density of the material without any pores.

There are different possibilities to measure material density and functional porosity. The Archimedes method (according to DIN EN 993-1 [16]) is a relatively simple procedure. For the determination of the material density and material porosity, the samples are weighted under air (m_1), then the samples have to be evacuated and in the next step intruded with liquid, for example, water (with the density ρ_{liq}), to fill open material pores. After the completed intrusion, the intruded samples are weighted underwater (m_2) and after careful dabbing off excess water (removal of drops from the surface) the sample mass is weighted in air (m_3). The material density of the struts can be calculated with the following equation:

$$\sigma_b = \frac{m_1}{m_3 - m_2} \cdot \rho_{liq} \tag{3}$$

and the open material porosity by

$$\pi_a = \frac{m_3 - m_1}{m_3 - m_2} \cdot 100 \tag{4}$$

The mercury intrusion porosimetry (MIP) represents a further option to measure the bulk density and open porosity as well as the pore size distribution using the intrusion of non-wetting mercury into the sample as a function of pressure. The bulk density and the apparent density are determined using measured volume values at the lowest pressure (bulk density) and highest pressure, for example, 420 MPa (apparent density). The material porosity of the struts is calculated by the ratio of bulk and apparent density. The pore size distribution is calculated by converting the pressure p in the corresponding pore radius r using the contact angle θ of mercury on the sample (140°) and surface tension γ (0.485 Nm^{-1}) of mercury [17]:

$$p = -\frac{2\gamma cos\theta}{r} \tag{5}$$

It has to be noted that the mercury intrusion porosimetry doesn't determine the true size of the pore cavities, but more the size of the entryways of the pores. Another possibility for an estimation of the pore size distribution is a microstructural analysis, e.g. with a scanning electron microscope (SEM). SEM is using a focused beam of primary electrons to produce images of a sample by scanning its surface. The electrons interact with atoms in the sample, producing signals containing information about materials contrast (backscattering electron mode) and surface topography (secondary electrons mode).

As the Al_2O_3 ceramic foams filters are used for the filtration of aluminum melt, properties at elevated temperatures are decisive as well. The thermal expansion can be measured by dilatometer or by apparatus for determining refractoriness under load while dilatometer records the length changes under a small force of around 30 cN, the apparatus for determining refractoriness under load uses higher load of 0.01 MPa to simulate operating conditions of refractories as close as possible to reality [18].

The chemical composition of the ceramic foams can be determined by, for example, XRF (X-ray fluorescence), EDX (Energy-dispersive X-ray spectroscopy), and ICP (Inductively coupled plasma). In this study, the EDX coupled with the SEM analysis was used which is able to analyze reliable elements with an atomic number larger than 10. Due to the limited irradiated area suitable for EDX point analyses, the variation in the measured elemental composition could be rather high, particularly in the case of inhomogeneous microstructure. Furthermore, the penetration depth of the primary electron beam depends on the material density.

Besides the chemical composition, the phase composition is of interest as well. X-ray diffractometry (XRD) uses X-rays which interact with the crystals of the samples and cause diffraction into many specific directions. By measuring the angles and intensities of the diffracted beams, the phases of the sample can be determined.

The examination of the mechanical properties, filter structure, different kinds of densities and porosities, microstructure, length change as a function of temperature, and elementary and phase composition of filters allow a profound assessment of the ceramic foam filters and help to predict their behavior and performance during metal melt casting. The mechanical properties might give a hint if the filter can survive the mechanical stresses of the primary melt impingement. The length change under temperature and load shows the ability to withstand higher temperatures. Elementary and phase compositions allow to estimate reaction with the aluminum alloy. Differences in the density, porosity, and composition between production batches might help to explain anomalies occurring during ceramic foam filter usage. The here mentioned ceramic foam properties do not allow predictions regarding the filtration efficiency.

Materials and Methods

Ceramic Foam Filters

The different above-mentioned material properties of the ceramic foams were measured on industrial Al_2O_3 foam filters with 30 ppi for continuous aluminum casting of five different producers named filter A, B, C, D, and E. The complete filters possessed a size of around 500 mm in square and a thickness of 50 mm. For the different measurements, different sample sizes were necessary. In the first step, cylindrical samples with a diameter of $\sim$50 mm were cut from the full-size filters with a diameter of 50 mm, using a diamond bit core drill attached to an EFB 152 PX tile drilling machine (Eibenstock, Germany) with water as the cooling medium. For smaller samples, the filters were cut using a diamond saw.

Mechanical Properties

The compressive strength was measured at room temperature on 20 cylindrical samples with a diameter of 50 mm and a height of 50 mm of each filter sample type. An 880 Hydraulic Tensile Testing Machine (MTS, USA) with loading plates with a diameter of 50 mm and a loading rate of 2 mm/min was used.

The Young's Modulus was determined by using the ultrasonic wave velocity method by measuring the transit time t with a BP-700 Pro (Ultratest GmbH, Deutschland). The sound propagation time of three samples was measured twice and Young's Modulus E was calculated with sample length s and the Poisson ratio μ:

$$E = \left(\frac{s}{t}\right)^2 \cdot \rho_{material} \cdot \frac{(1-2\mu)(1-\mu)}{1-\mu} \tag{6}$$

Structural Properties

The foam density was calculated by measuring the weight and the dimensions of the foam of 20 foam samples per sample type.

The porosity of the filter, the functional pore size, and the strut thickness was quantified with a microfocus X-ray computer tomograph CT-ALPHA (ProCon XRay, Germany) equipped with a 160 kV X-ray tube and a Dexela 1512 detector (Perkin Elmer, Germany) with 1944 × 1526 active pixels. One filter sample per filter type with a diameter of 50 mm and a height of 50 mm was acquired. The software package Modular Algorithms for Volume Images MAVI (Fraunhofer ITWM, Kaiserslautern, Germany) was used for the image data processing consisting of a cropping step, followed by a binarization with Otsu's threshold, and a morphological operation "closing" for the closure of the polyurethane pores followed by the elimination of the polyurethane pores by a labeling and object filter procedure. Additionally, the strut thickness of at least 30 struts per filter type was measured with a digital microscope VHX-2000D (Keyence, Japan). The microstructure was evaluated at grinded and polished microsections with a scanning electron

microscope Philips XL 30 (Philips, Germany) equipped with an energy-dispersive X-ray microanalysis device (Phoenix, USA).

Physical Properties

The Archimedes procedure was evaluated for bulk samples, but its application to ceramic foam filters is a challenging task due to the following difficulties. Firstly, due to the sample transfer from the immersion liquid bath to the balance, air bubbles in the ceramic foam samples are created, and therefore the sample weight is not measured correctly. The air bubbles could be removed by vibrating the sample in the immersion liquid. Secondly, a careful dabbing off water drops from the sample surface is not possible by wiping. For the removal of water drops from the ceramic foam surface, the usage of a centrifuge provided repeatable results. It should be noted that the speed of the centrifuge should be chosen with caution for the avoidance of a liquid removal from the pores and breakage of struts. For the application of a centrifuge, a sufficient ceramic foam strength is required which was not the case for filter B. The rotation caused the failure of the samples. For every filter type, 3–4 samples were measured with a size of around $40 \times 40 \times 10$ mm^3.

The mercury intrusion porosimetry measurements with an Autopore 5 (Micromeritics, USA) used evacuation to a pressure of <50 µm Hg before the penetrometer was filled with mercury. The starting intrusion pressure was set to 0.005 MPa and the measurement was performed with an equilibrium time of 5 s. Two measurements per filter sample type were performed at samples with around $10 \times 10 \times 10$ mm^3.

The true density was measured twice for every filter type with a helium pycnometer AccuPyc 1340 TEC (Micromeritics, USA). Previously, the ceramic foam samples were ground to a size smaller than 63 µm to eliminate the closed pores.

Thermal Properties

The dilatometry was performed using a dilatometer DIL 402 C (Netzsch, Germany) carried out under air with 5 K/min to a temperature of 1000 °C. Samples were cut with a diamond saw in samples of around $8 \times 8 \times 20$ mm^3. The measurements with the apparatus for determining refractoriness RUL/CIC 421 (Netzsch, Germany) were conducted at a load of 100 N and a heating rate of 5 K/min to a temperature of 1600 °C. The cylindrical samples with a diameter of 50 mm and a height of 50 mm were used.

Chemical and Phase Composition

The EDX analysis was conducted at two to three positions with a size of at least 400×200 µm^2. For comparable results, the measuring time was approximately the same. The detection limit of elements with an atomic number ≥ 10 is around 0.1 mas%. For an easier interpretation, the measured amounts are presented as oxides.

For the XRD measurement, the ceramic foam filters were ground to a size <63 µm. The measurements were conducted with an XRD X'Pert Pro MPD (Malvern PANalytical, Germany) in the angle range of 7.5–90°. The software Highscore (Malvern PANalytical, Germany) was used for the evaluation of the phase composition starting with the removal of the underground, searching for reflexes, and search and comparison of possible phases. The detection limit is 1 vol% for crystalline phases.

Results

Mechanical Properties

The mechanical properties are presented in Table 1. The compressive strength ranged between 0.88 and 1.50 MPa and Young's Moduli between 10.0 and 18.1 GPa. There are significant differences between the different ceramic foam filters. No correlation between the compressive strength and Young's Modulus was detectable.

Structural Properties

The functional porosity of the different sample types was between 73 and 80%, see Table 2. The strut thickness was evaluated by the open foam feature of the software MAVI and digital microscope.

The CT method delivers significantly larger values than the measurements by the digital microscope, whereby the results of the digital microscope are more reliable. Although the CT measurements analyze all struts of the scanned sample, the digital microscope only 30–40 struts have been analyzed. Furthermore, with the digital microscope, the thickness of the strut at the thinnest point is measured whereby the CT analysis used a larger region of the strut. The differences in the strut diameter might be reduceable on the number of closed pores in the ceramic foam filters visible in Fig. 1. The closed pores enlarge the determined strut diameters analyzed by CT.

The mean diameter of the pores determined by the open foam features is larger than analyzed by the feature complex

Table 1 Compressive strength of the different filter types

	Compressive strength/MPa	Young's modulus/GPa
Filter A	1.27 ± 0.16	13.0 ± 0.8
Filter B	1.05 ± 0.12	18.1 ± 1.0
Filter C	0.88 ± 0.13	10.0 ± 0.8
Filter D	1.37 ± 0.13	11.3 ± 0.7
Filter E	1.50 ± 0.18	16.7 ± 1.9

Table 2 Structural properties of the different filter types

Properties	Functional porosity/%	Mean diameter of the struts/mm	Mean strut thickness/mm	Mean diameter of the functional pores/mm	
Method	CT field feature	CT Open foam feature	Digital microscope	CT Open foam feature	CT complex morphology
Filter A	80	0.54	0.32 ± 0.11	3.76	2.58 ± 0.30
Filter B	79	0.75	0.34 ± 0.05	4.78	3.25 ± 0.43
Filter C	75	0.72	0.29 ± 0.06	3.93	2.24 ± 0.30
Filter D	73	0.69	0.34 ± 0.07	4.13	2.77 ± 0.37
Filter E	79	0.56	0.29 ± 0.07	3.74	2.59 ± 0.31

morphology. For the analysis with the feature complex morphology, more than 3700 pores were analyzed. The large standard deviation between 11 and 14% shows the high inhomogeneity of the pore diameter typical for reticulated ceramic foam filters.

Besides the evaluation of functional pore size, the material pores play an important role in the thermomechanical properties. SEM images of microsections of the struts provide information of the material microstructure. The five different filter types showed large differences, see Fig. 1a, d, g, j, m. The filters A, B, and E possessed homogenous small pores, whereas Filter C and D had a broad pore size distribution and inhomogeneously distributed pores.

Physical Properties

The foam densities were between 0.33 and 0.41 g/cm^3 whereby filter C possessed a significantly lower foam density than the other filters, see Table 3. The differences of the bulk densities determined by Archimedes method and by mercury intrusion porosimetry are within the standard deviation except for filter E which showed a higher value for the mercury intrusion porosimetry measurement, see Table 3.

The differences for the open material porosity were significantly larger whereby the values determined by mercury intrusion porosimetry were smaller than values determined by Archimedes method for filter A, B, D, and E. This is explainable with differences between the Archimedes procedure and the mercury intrusion porosimetry. Archimedes uses a wetting liquid (e.g. water) and so a wetting of the sample and filling the pores and strut cavities take place before the measurement of the bulk density. In contrast, mercury intrusion porosimetry uses non-wetting mercury which has to be forced by the application of pressure to fill the pores and the strut cavities whereby at the moment of the measurement of the bulk density, the strut cavities are not filled with mercury yet. Thus, the volume of strut cavities is included in the open porosity for Archimedes but excluded for the mercury intrusion porosimetry. For filter C, the values determined by mercury intrusion porosimetry were larger which can not be explained yet.

The pore size distribution measured by mercury intrusion porosimetry does not correspond to the real material pores but more to the pore entryway distribution due to the intrusion of larger pores in the sample center at higher pressures because the smaller entryways positioned in the outer areas of the sample has to be intruded before. The cumulative pore volume in dependent on the pore entryway diameter showed two strong increases of the cumulative mercury volume, see Fig. 2. The first increase corresponds to the filling of the strut cavities [13], whereas the second increase corresponds to the mercury filling of the material pores. The filters A, B, and E show a comparable progression of the cumulative volume.

Filters C and D show a different progression with an increase of the cumulative volume at larger pores than Filters A, B, and E, which is consistent with the corresponding SEM images.

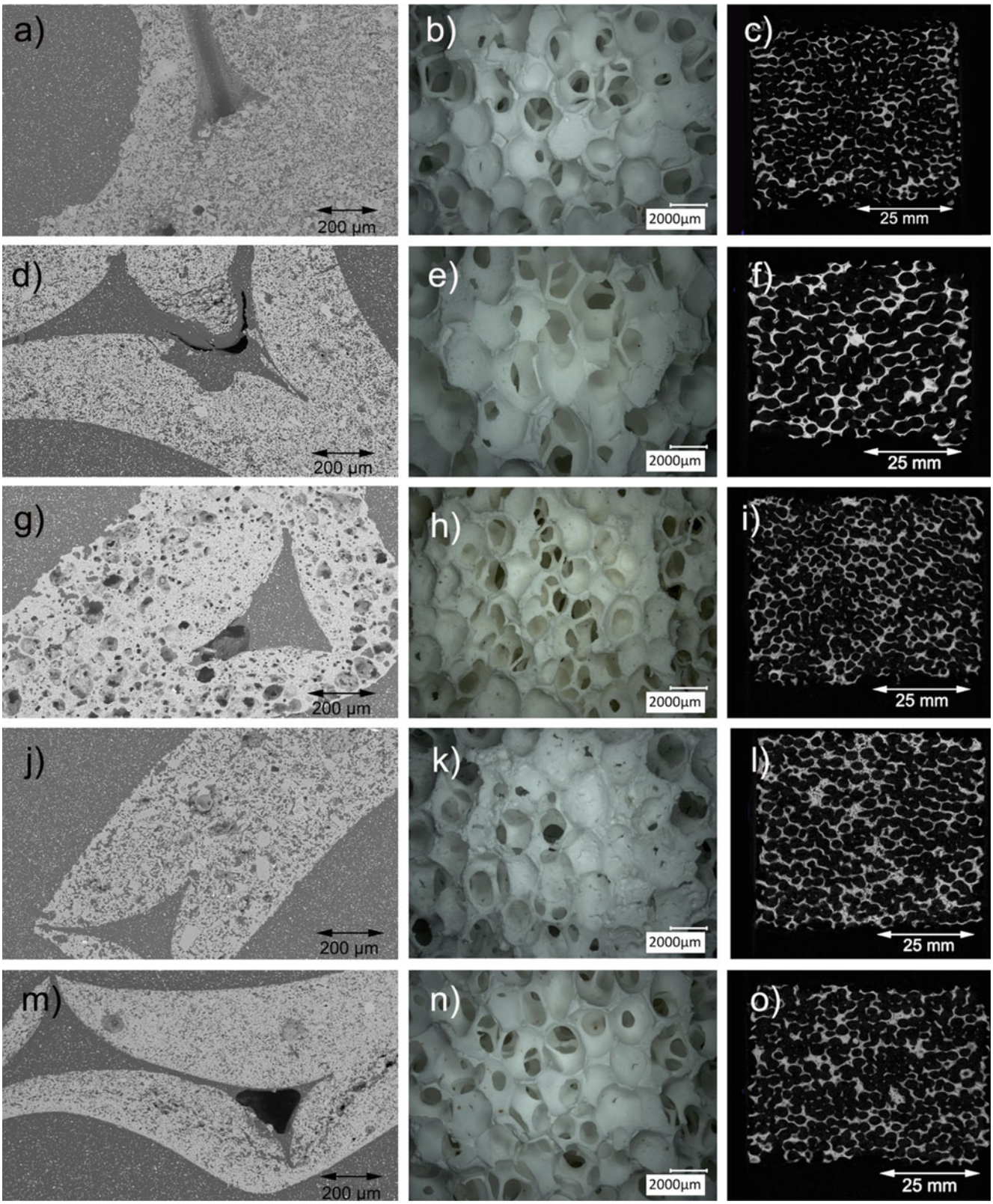

Fig. 1 Morphology of the filters, left column shows the SEM images, middle row the digital microscope images, and right column CT images, Filter A (**a**, **b**, **c**), Filter B (**d**, **e**, **f**), Filter C (**g**, **h**, **i**), Filter D (**j**, **k**, **l**), and Filter E (**m**, **n**, **o**)

Table 3 Densities and porosities of the different filter types

	Foam density/g/cm^3	Bulk density/g/cm^3		Open material porosity/%		True strut density/g/cm^3	Relative density
		Archimedes method	Mercury intrusion porosimetry	Archimedes method	Mercury intrusion porosimetry	Helium pycnometry	
Filter A	0.41 ± 0.02	1.98 ± 0.05	2.09 ± 0.04	43.06 ± 0.96	41.08 ± 5.51	3.58 ± 0.01	0.21
Filter B	0.40 ± 0.01	2.01 ± 0.09	2.03 ± 0.03	43.48 ± 5.42	38.09 ± 2.86	3.50 ± 0.01	0.20
Filter C	0.33 ± 0.01	1.68 ± 0.01	1.78 ± 0.02	39.67 ± 0.89	47.02 ± 1.11	2.95 ± 0.01	0.20
Filter D	0.39 ± 0.01	1.70 ± 0.09	1.74 ± 0.07	49.09 ± 3.20	34.13 ± 1.66	3.49 ± 0.01	0.23
Filter E	0.41 ± 0.02	1.97 ± 0.06	2.15 ± 0.02	40.85 ± 2.32	37.83 ± 0.26	3.52 ± 0.01	0.21

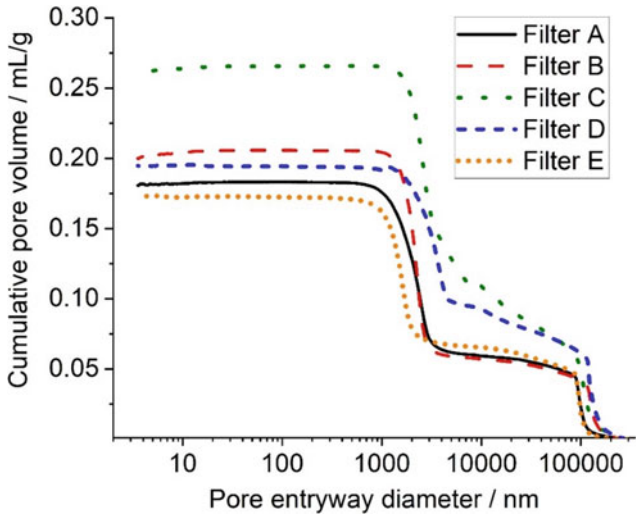

Fig. 2 Cumulative pore volume in dependence on the pore entryway diameter of the filters measured with mercury intrusion porosimetry

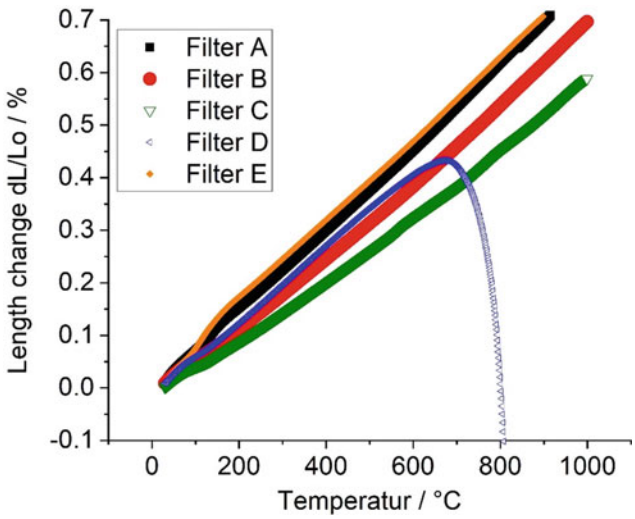

Fig. 3 Length change in dependence on the temperature (dilatometer measurements). (Color figure online)

The thermal expansion measured by dilatometry is presented in Fig. 3. Filters A, B, C, and E showed a linear increase with small differences in the slope of the curve corresponding to the coefficient of thermal expansion whereby filter C possessed the lowest coefficient of thermal expansion followed by filter B, see Table 4. It has to be noted that only one measurement per filter type was conducted except filter D which was measured twice due to the divergent behavior. Filter D possessed a strong decrease in the length starting from around 640 °C caused probably by melting of present phases.

The results of the measurements with the RUL apparatus are consistent with the dilatometry measurements for filter D and showed also a strong length change at temperatures at 650 °C, see Fig. 4. A softening of the filters A, B, C, and E was observable as well but at significantly higher temperatures increasing in the order filter C, filter A, filter B, and filter E.

Chemical and Phase Composition

The partially large standard deviation presented in Table 5 (for example, filter C) was probably caused by different phases in the struts which is consistent with the SEM image of filter C (Fig. 1g) showing inhomogeneities.

The chemical compositions of the filter types show that filters A and E were phosphate bonded Al_2O_3, whereas filters B, C, and D were phosphate-free filters gaining importance due to the formation of toxic phosphine gas (PH_3) during the contact of aluminum melt (with Mg) and phosphate bonded Al_2O_3 ceramic foam filters [19, 20].

Table 4 Coefficient of thermal expansion of the different filter types

Filter type	Coefficient of thermal expansion/10^{-6} K^{-1}	Measuring range
Filter A	7.78	between 100 and 1000 °C
Filter B	7.09	between 100 and 1000 °C
Filter C	6.05	between 100 and 1000 °C
Filter D	7.08	between 100 and 600 °C
Filter E	7.75	between 100 and 1000 °C

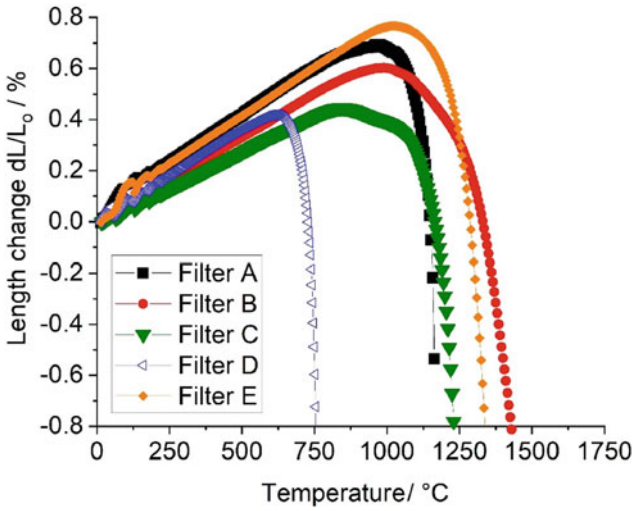

Fig. 4 Length change in dependence on the temperature (RUL apparatus). (Color figure online)

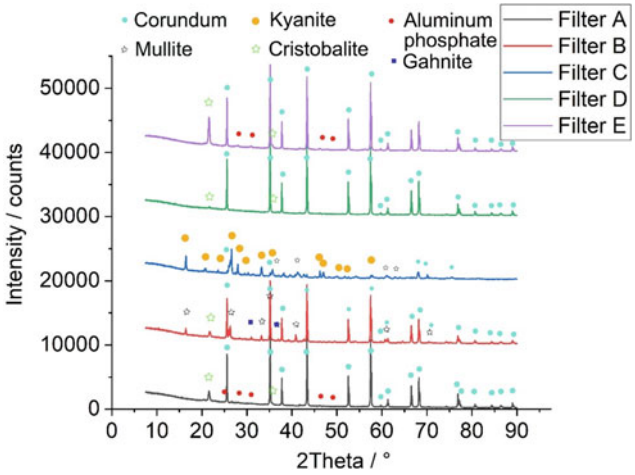

Fig. 5 Diffractograms of the different filter types. (Color figure online)

Table 5 Chemical composition of the different filter types

	Al_2O_3	SiO_2	P_2O_5	Na_2O	K_2O	MgO	CaO	ZnO	TiO_2	Fe_2O_3
Filter A	80.9 ± 6.2	13.6 ± 4.9	4.5 ± 1.3	0.5 ± 0.03	0.5 ± 0.1					
Filter B	78.2 ± 1.6	21.0 ± 1.5		0.3		0.5				
Filter C	73.4 ± 10.2	24.0 ± 10.1	<0.1	0.4 ± 0.2	0.3		0.8	1.0		
Filter D	50.1 ± 0.6	46.0 ± 0.5	<0.1	0.2			2.4		0.8	0.6
Filter E	88.2 ± 3.3	2.3 ± 0.3	9.4 ± 3.0	0.3						

According to patents of the phosphate-free ceramic foam filters [21, 22], a borate glass frit can be used as binder phase. Boron is due to its atomic number of 5 not detectable by EDX.

The results of the XRD measurements are presented in Fig. 5. For the identification of the phases from the XRD measurement, the software Highscore proposes different possible phases whereby a definite allocation is often difficult. Furthermore, a basic requirement is the availability of the phases in the used database.

The identified phases were mainly corundum (Al_2O_3) for filters A, B, D, and E. The phosphate bonded filters (filtesr A and E) contained small amounts of aluminum phosphate ($AlPO_4$) confirmed also by EDX (Table 5). In filters B and C, mullite ($3Al_2O_3{\cdot}2SiO_2$) was detected. Cristobalite (SiO_2) was found in the filters A, D, and E. In filter D, gahnite ($ZnAl_2O_4$) was detected. Filter C showed a different phase composition in comparison to the other filters with the main crystal phase kyanite (Al_2SiO_5). Furthermore, the measured intensity was significantly lower caused probably by a lower degree of crystallinity. Filter C possessed the lowest coefficient of thermal expansion of the five filters due to a large amount of kyanite having a smaller coefficient of thermal expansion than corundum.

Conclusion

The study showed practicable possibilities and limitations of the characterization of ceramic foam filters. The list do not claim to be complete. The compressive strength and Young's Modulus were measured and showed significant differences between the different filter types. For the evaluation of the foam structure, the functional pore size and strut thickness were determined. Furthermore, the foam density, bulk density, true density, relative density, and open material porosity were measured. The entryway size distribution within the struts was calculated from the mercury intrusion porosimetry measurements. With the help of length change measurements in dependence on the temperature, the coefficient of thermal expansion and the maximum operating temperatures were determined. The analysis of the chemical and phase composition of the five filter types round off this study.

The discussed properties can be used for the development of new filter compositions, for the choice of appropriate ceramic foam filter or for troubleshooting in the case of problems. In dependence on the targeted problem, the suitable measurement methods should be chosen, whereby the limitations of the methods should be taken into consideration.

Acknowledgements The authors would like to thank the German Research Foundation (DFG) for supporting these investigations as part of the Collaborative Research Centre 920 "Multi-Functional Filters for Metal Melt Filtration—A Contribution towards Zero Defect Materials" (Project-ID 169148856) sub-projects A02 and S01.

References

1. Brown JR (1999) Foseco Non-Ferrous Foundryman's Handbook, Butterworth Heineman, ISBN 0 7506 4286 6: 99–107
2. Brown JR (2000) Foseco Ferrous Foundryman's Handbook, Butterworth Heineman, ISBN 0 7506 4286 6: 245–295
3. BDG-Richtlinie (VDG Merkblatt) P100 (2012) Keramische Filter in Schaumstruktur – Schaumkeramikfilter für Eisen- und Stahlguss. October 2012
4. Standard DIN EN ISO 8895 (2006) Shaped insulating refractory products – Determination of cold crushing strength
5. Standard DIN EN 993–5 (1998) Methods of test for dense shaped refractory products—Part 5: Determination of cold crushing strength
6. Brezny R, Green DJ (1993) Uniaxial strength behavior of brittle cellular materials. J. Am. Ceram. Soc. 76(9): 2185–2192
7. Wolf S, Walther H, Langer P, Stoyan D (2008) Statistische Untersuchungen der Druckfestigkeit von Porenbeton – Größeneffekt und Umrechnungsfaktoren. Mauerwerk 12 (1): 19–24
8. Dam CQ, Brezny R, Green DJ (1990) Compressive behavior and deformation-mode map of an open cell alumina. J. Mater. Res. 5 (1): 163–171
9. Oliveria FAC, Dias A, Vaz MF, Fernandes JC (2006) Behavior of open-cell cordierite foams under compression. J. Eur. Ceram. Soc. 26(1-2) 179–186
10. Emmel M, Aneziris CG (2012) Development of novel carbon bonded filter compositions for steel melt filtration. Ceram. Int. 38 (6): 5165–5173
11. Voigt C, Storm J, Aneziris CG, Abendroth M, Kuna M, Hubálková J (2013) The influence of the measurement parameters on the crushing strength of reticulated ceramic foams. Mater. Res. 28 (17): 2288–2299
12. Grabenhorst J, Luchini B, Fruhstorfer J, Voigt C, Hubálková J, Chen J, Li N, Li Y, Aneziris CG (2019) Influence of the measurement method and sample dimensions on the Young's modulus of open porous alumina foam structures, Ceram. Int. 45 (5): 5987–5995
13. Voigt C, Hubalkova J, Ditscherlein L, Ditscherlein R, Peuker U, Giesche H, Aneziris CG (2018) Characterization of reticulated ceramic foams with mercury intrusion porosimetry and mercury probe atomic force microscopy. Ceram. Int. 44 (18): 22963–22975
14. Adler J, Standke G (2003) Offenzellige Schaumkeramik. Teil 1. Keram. Z. 55 (9): 694–703
15. Standard ASTM D3576 (2004) Test Method for Cell Size of Rigid Cellular Plastics
16. Standard DIN EN 993-1 (2018) Methods of test for dense shaped refractory products—Part1: Determination of bulk density. apparent porosity and true porosity
17. Giesche H (2002) Mercury Porosity. Handbook of Porous Solids 1, Wiley-VCH. 309–351
18. Standard DIN EN 993–8 (1997) Methods of testing dense shaped refractory products—Part 8: Determination of refractoriness-underload
19. Aubrey LS, Olson R, Smith DD (2009) Development of a phosphate—Free reticulated foam filter material for aluminum Cast Houses. Mater. Sci. Forum. 630: 137–146
20. Solem CKW, Fritzsch R, Aune R.E (2018) Preliminary experimental study of the thermal stability and chemical reactivity of the phosphate-based binder used in Al_2O_3-based ceramic foam filters. Extraction: 1153–1163.
21. Chi F, Haack DP, Aubrey LS (2013) Low expansion corrosion resistant ceramic foam filters for molten aluminum filtration. US Patent 8518528 B2
22. Vincent M (2019) Ceramic filter for non-ferrous metals. US Patent 2019/0240605 A1.